Structural Changes of Poly(trimethylene terephthalate) Film upon Uniaxial and Biaxial Drawing

Han Sup Lee* and Su Cheol Park

Department of Textile Engineering, Inha University, 253 Yong-Hyun-Dong, Inchon 402-751, Korea

Young Ho Kim

Department of Textile Engineering, Soongsil University, Seoul 156-743, Korea

Received May 18, 1999; Revised Manuscript Received January 3, 2000

ABSTRACT: Structural changes occurring during a stretching process have been studied with the uniaxially and biaxially drawn PTMT films. The stress-induced crystallization has been observed from the stress−strain curve showing abrupt increase of stress at a specific draw ratio (dr = 2.5) at which the density was found to increase significantly with the draw ratio. This stress-induced crystallization phenomenon was also confirmed with the decreased crystallization enthalpy and increased glass transition temperature approximately at dr = 2.5. The refractive indices along three principal directions were also measured with the polarized refractometer. It was found that for the uniaxially drawn films the refractive index along the deformation direction showed fast increase at the onset of stress-induced crystallization. Using double-edged ATR crystal and rotatable sample holder, the orientation parameters of several infrared bands along three spatial directions of PTMT films were obtained with the polarized FTIR-ATR spectroscopy. By normalizing absorbances of all infrared bands studied in this work with absorbance of the reference band at 1410 cm^{-1}, followed by multiplying the absorbance of TM polarization with the theoretical effective thickness ratio between two polarizations, i.e., d_e(TE)/d_e(TM), attenuation indices in three principal directions were found to be very close to each other for samples prior to drawing. In general, attenuation indices along the deformation directions increased with the increasing function of draw ratio for the bands of which transition moments are parallel to the chain direction. The fact that the attenuation index of the band at 1358 cm^{-1} showed an abrupt increase at dr = 2.5 indicates that this band is preferentially affected by the trans conformers in the crystalline region. All three attenuation indices of the 1385 cm^{-1} band that corresponds to the CH_2 wagging mode of gauche conformers showed a gradual decrease with the draw ratio, probably due to the conformation change upon stress-induced crystallization. The orientation parameters along the deformation directions of the C−O stretching band at 1040 cm^{-1} increased almost continuously without sudden jump at the onset of stress-induced crystallization.

Introduction

Aromatic polyesters such as poly(ethylene terephthalate) (PET), poly(trimethylene terephthalate) (PTMT), and poly(butylene terephthalate) (PBT) show a so-called odd−even effect depending on the number of the methylene units between two adjacent aromatic rings.[1] Since PTMT has an odd number of methylene units, it shows different and characteristic properties such as high breaking strain and elastic recovery, compared with PET and PBT which have even number of methylene units.[2] Whereas PET and PBT have been extensively studied theoretically as well as experimentally and used for a variety of applications, studies on PTMT and its industrial application have been relatively limited. Even though there have been several reports on the various aspects of PTMT,[2−9] a more extensive study on PTMT has to be still carried out to completely understand basic properties and expand an applicability of this material.

Physical properties of a polymer are determined not only by the chemical structure but also by the internal morphology such as the degree of crystallinity and orientation. Infrared spectroscopy has been widely used for the study of a segmental orientation, because it gives selective information on the orientation of each segment in a polymeric chain. Furthermore, information on conformational change and formation of crystalline structure can be also easily obtained through the infrared spectroscopy. However, most commercial polymeric films and fibers are too thick to be studied with the transmission infrared method. Spectroscopic methods such as specular reflection and attenuated total reflection (ATR) can be the useful alternatives.[10−22]

The FTIR-ATR method is frequently used for the structural characterization of surfaces of thick polymer films, fibers, fabrics, and coatings, because absorption occurs mainly at the surface of the sample.[12−22] One of the most important aspects of the FTIR-ATR method is that the electric field of the evanescent wave exists in all three spatial directions in the rarer medium. Therefore, orientation information along three spatial directions can be obtained with the FTIR-ATR method.[13−17]

In this work, segmental orientation and morphology changes occurring during the uniaxial and biaxial deformation of PTMT films have been studied with the polarized FTIR-ATR method. The orientation of polymeric chains along three directions was also investigated by measuring three principal refractive indices with the polarized refractometry. The results on segmental and chain orientations were also compared with the structural changes observed through the density and DSC measurement.

* To whom all correspondence should be addressed.

10.1021/ma990775w CCC: $19.00
Published on Web 09/30/2000

Table 1. Selective IR Band Assignment of PTMT

wavenumber (cm^{-1})	assignment
1410	aromatic ring vibration
1385 (∥)[a]	CH_2 wagging vibration (gauche conformer)
1358 (∥)	CH_2 wagging vibration (trans conformer)
1040 (∥)	C−O stretching vibration (asym)

[a] ∥: The direction of transition dipole moment vector is parallel to chain axis.

Experimental Section

Sample Preparation. The sample studied in this work was poly(trimethylene terephthalate) polymerized from terephthalic acid and 1,3-propanediol, with the intrinsic viscosity of 0.84 dL/g in dichloroacetic acid at 30 °C. The PTMT polymer chips were heated approximately to 245 °C to ensure homogeneous and amorphous state (T_m = 225 °C)[1] and pressed into a thin film (~300 μm in thickness) using a hot press, followed by quenching into an ice−water to prevent crystallization. The melt-quenched amorphous PTMT films were then stretched uniaxially or biaxially using biaxial stretcher at 55 °C (T_g = 35 °C)[1] with 10%/s strain rate. For the biaxial drawing, drawing was done simultaneously in both directions with the same draw ratios along the two directions (MD's, machine directions). Uniaxial drawing was done with the same setup as biaxial drawing, keeping the width of the sample (along TD, transverse direction) constant during the drawing along MD. Immediately after drawing, the drawn films were cooled below the glass transition temperature of PTMT before the drawn films were demounted from the biaxial stretcher by blowing cold air to minimize the orientation relaxation and crystallization.

Measurements. FTIR-ATR spectra were obtained with the Nicolet 520p FTIR spectrometer equipped with a liquid nitrogen cooled MCT detector at 2 cm^{-1} resolution using the ATR setup developed initially by Sung and co-workers, which consisted of symmetrically double-edged parallelogram KRS-5 crystal (25 × 25 × 3 mm, 45° cut, Harrick Scientific) and rotatable sample holder.[14,15] Polarized infrared radiation was available by placing the wire-grid polarizer (Harrick Scientific) between the ATR setup and detector. To obtain orientation information along all three directions (MD, TD, ND for uniaxial drawing and MD, MD, ND for biaxial drawing), four FTIR-ATR spectra were collected by rotating the polarizer and film by 90°.[13−17] Depending on the direction of polarizer and sample, four coordinates such as TE,*x*, TM,*x*, TE,*y*, and TM,*y* are available. In the TE,*x* coordinate, for example, the machine direction (of uniaxially drawn sample) is parallel with the electric field direction which is perpendicular to the plane of incidence. The assignment of infrared bands used in this work for the quantitative analysis is shown in Table 1.[24,25] Absorbances of infrared bands at 1410, 1385, and 1358 cm^{-1} were obtained from peak areas after curve fitting, and the absorbance value for 1040 cm^{-1} was obtained from peak height above the local baseline.

Three principal refractive indices of drawn films were measured with the polarized refractometer (Atago, Abbe refractometer 4T) using a sodium lamp (λ = 589 nm). Methylene iodide (n = 1.74) was used as a contact liquid in order to provide a continuous path for the light by excluding air between the prisms and sample. Density of the drawn films was measured with a density gradient column at room temperature using carbon tetrachloride (d = 1.59 g/cm^3) and toluene (d = 0.87 g/cm^3). The glass transition temperature and enthalpy of crystallization were obtained from thermograms obtained with a Shimazu DSC-50 at 10 °C/min heating rate, and the stress−strain curve was measured with the load cell (LC1205-K020, A&D Co. Ltd.) and strain gauge (PY2F50S300, Gefran Sensori Co. Ltd.) in the temperature-controlled mechanical stretcher built in this laboratory.

ATR Analysis. From four infrared absorbances ($A_{TE,x}$, $A_{TM,x}$, $A_{TE,y}$, $A_{TM,y}$) of a selected band in four spectra obtained experimentally, three spatial attenuation indices (k_x, k_y, k_z) along three principal directions in a film can be calculated using eq 1.[13]

$$A_{TE,x} = \alpha k_x \tag{1a}$$

$$A_{TM,x} = \beta k_y + \gamma k_z \tag{1b}$$

$$A_{TE,y} = \alpha k_y \tag{1c}$$

$$A_{TM,y} = \beta k_x + \gamma k_z \tag{1d}$$

Here, α, β, γ defined in eq 2 are functions of the angle of incidence (θ) and refractive indices of the sample ($\bar{n}_{polymer}$) and ATR crystal ($n_{crystal}$).

$$\alpha = \frac{4n^2 \cos\theta}{(\sin^2\theta - n^2)^{1/2}(1 - n^2)} \tag{2a}$$

$$\beta = \frac{4n^2 \cos\theta(\sin^2 - n^2)}{(\sin^2\theta - n^2)^{1/2}(\sin^2\theta - n^2 + n^4\cos^2\theta)} \tag{2b}$$

$$\gamma = \frac{4n^2 \cos\theta \sin^2\theta}{(\sin^2\theta - n^2)^{1/2}(\sin^2 - n^2 + n^4\cos^2\theta)} \tag{2c}$$

$$n = \frac{\bar{n}_{polymer}}{n_{crystal}} \tag{2d}$$

Equation 1 has been developed assuming that the refractive indices along three principal directions are the same, i.e., $n_x = n_y = n_z = \bar{n}_{polymer}$.[13−17] If three principal refractive indices become different from each other upon deformation of the sample, the orientation information calculated with eqs 1 and 2 may contain a small amount of approximation error. It is, however, impractical to consider the variation of the refractive indices along all three directions upon drawing when attenuation indices (k_x, k_y, k_z) are calculated with eqs 1 and 2. In this study, the average refractive index of PTMT film (n = 1.58) was obtained with amorphous and isotropic samples at 589 nm wavelength. That of KRS-5 crystal is 2.37.[23] Using these refractive indices and a 45° angle of incidence, α, β, and γ were calculated to be 9.15, 1.94, and 16.37, respectively.

The absorbances of IR bands in polarized ATR spectra are extremely sensitive to the nature of the optical contact between the sample and ATR crystal as well as effective thickness. To solve these problems, the band ratioing technique using the reference band at 1410 cm^{-1} (aromatic ring vibration band) was used.[18] That band is a well-established reference band in the case of PET.[17−19] The independence of that band on the orientation was verified again with the PTMT sample with the transmission infrared dichroism measurement in this work. The intensity of that band was also observed not to change abruptly during the crystallization and melting of the crystal, which was again verified in this work with the transmission infrared method equipped with a heating accessory.

When using the band ratioing method, the effective thickness difference between two waves has to be considered carefully. The effective thickness of the TE (transverse electric) and TM (transverse electric) wave is a function of refractive indices of sample and ATR crystal, angle of incidence, and wavelength of IR radiation, as shown in eq 3.[12]

$$\frac{d_e(TE)}{\lambda_1} = \frac{n\cos\theta}{\pi(1 - n^2)(\sin^2\theta - n^2)^{1/2}} \tag{3a}$$

$$\frac{d_e(TM)}{\lambda_1} = \frac{n\cos\theta(2\sin^2\theta - n^2)}{\pi(1 - n^2)[(1 + n^2)\sin^2\theta - n^2](\sin^2\theta - n^2)^{1/2}} \tag{3b}$$

$$\lambda_1 = \lambda/n_{crystal} \tag{3c}$$

It is noted from eq 3 that effective thickness of the TM wave

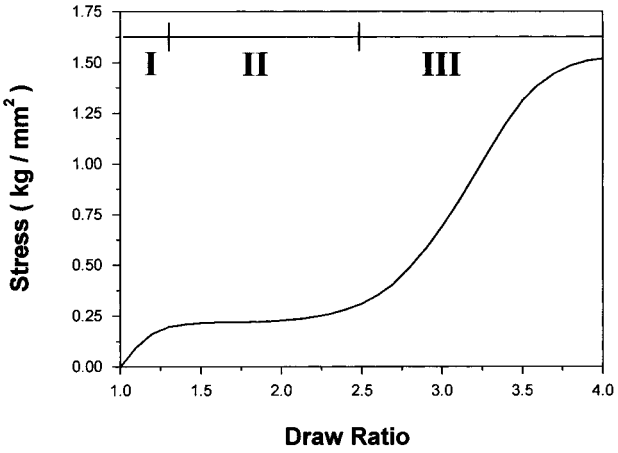

Figure 1. Stress−draw ratio curve of melt-quenched amorphous PTMT film during uniaxial drawing at 55 °C.

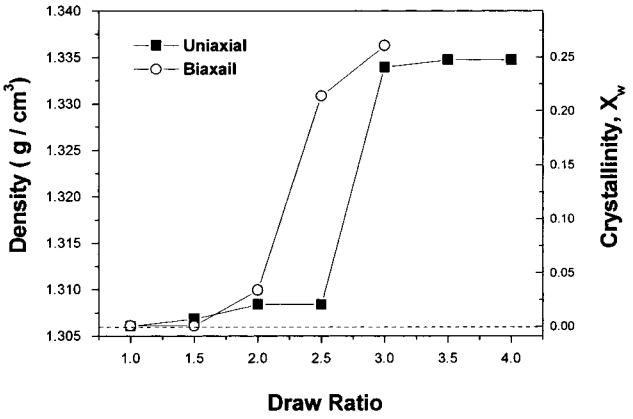

Figure 2. Density changes as a function of draw ratio for uniaxially and biaxially drawn PTMT films. Crystallinity is plotted with a right ordinate.

is always greater than that of the TE wave. At a 45° angle of incidence, the ratio of effective thickness of TM to that of TE is 2, i.e., $d_e(\mathrm{TE})/d_e(\mathrm{TM})$. This indicates that the ratio of absorbance of the TM wave to that of the TE wave in eq 1 should be 2 for the isotropic sample, i.e., $A_{TE}/A_{TM} = 2$. In this work, all absorbances were normalized with the absorbance of the reference band. Since the inherent difference between the absorbances of two polarized radiations (TM and TE waves) was removed by the normalization process, the absorbance of the TM wave was then multiplied with the theoretical ratio, 2, prior to the calculation of attenuation indices with eq 3. The absorbance difference between two waves obtainable after multiplication with the $d_e(\mathrm{TE})/d_e(\mathrm{TM})$ ratio is then expected to be solely due to the dichroic effect.

The structural factor (A_0) defined below is the average value of three attenuation indices.[17]

$$A_0 = \frac{1}{3}(k_x + k_y + k_z) \tag{4}$$

The structural factor is independent of orientation of the sample and proportional to the total concentration of a functional group related to the corresponding infrared band. The relative distribution of attenuation indices along three directions(x, y, z) can be expressed with spatial orientation parameters (A'_x, A'_y, A'_z).[17]

$$A'_x = k_x/A_0 \tag{5a}$$

$$A'_y = k_y/A_0 \tag{5b}$$

$$A'_z = k_z/A_0 \tag{5c}$$

For an isotropic sample, all three spatial orientation parameters have the value of one. In the case of uniaxially drawn and perfectly oriented sample, the attenuation indices along the y, z directions of an infrared band of which the transition moment vector is exactly parallel with the chain direction will become zero. And, the spatial orientation parameter in the x direction will be 3. The spatial orientation parameters along the deformation directions will be 1.5 for the above infrared band in a perfectly oriented, biaxially drawn sample. Since the range of spatial orientation parameter is well-defined, the relative degree of orientation along three principal directions can be estimated from absolute values of spatial orientation parameters obtained experimentally.

Results and Discussion

Stress−Draw Ratio Curve. To understand the structural change during the drawing process, the stress−strain curve (stress−draw ratio curve) of a melt-quenched amorphous PTMT film was measured at 55 °C and shown in Figure 1. The overall curve can be divided into three regions as denoted in the figure. In region I, the stress increases almost linearly with the increasing draw ratio. As the film is deformed during this region, the amount of entanglements between polymer chains in the amorphous region is known to decrease through the rotation and slip of the chains.[26] In region II between draw ratio 1.25 (dr = 1.25) and 2.5, the stress remains almost constant. The polymer chains free from chain entanglements tend to flow and align along the deformation direction. And, the chain segments between two adjacent entanglement points may undergo stretching during this period. A further increase of the draw ratio above 2.5 causes a significant strain hardening as shown in region III. The fast increase of the modulus in this region indicates that there might be major structural changes occurring in addition to the orientation of the chain along the deformation direction.

Stress−strain curves of amorphous PET have also been measured at various temperatures above the glass transition temperature of PET.[27,28] Even though the actual shape of stress−strain curves changed depending on the drawing temperature, the basic structures such as abrupt increase of stress in region I, plateau region in region II, and strain hardening in region III were maintained.

Density Measurement. In Figure 2, the density of uniaxially/biaxially drawn films is plotted as a function of draw ratio. The mass fraction crystallinity (X_w) is also shown with the right ordinate. The density of an ideal crystal was reported to be 1.43 g/cm^3, and the density of the melt-quenched amorphous PTMT measured in this work was 1.306 g/cm^3, which was used as the density of pure amorphous PTMT to calculate X_w.[5]

The density of the samples drawn uniaxially or biaxially increases with the increase of the draw ratio, indicating that the strain-induced crystallization occurs during drawing. For the uniaxially drawn samples, the density remains almost constant until the draw ratio reaches about 2.5, at which an abrupt density increase is observed. Further increase of the draw ratio above dr = 3.0 does not change the density noticeably. In the case of biaxially drawn samples, the major strain-induced crystallization starts to occur at about dr = 2.0, which is slightly lower than the corresponding value for uniaxially drawn samples. Since the thickness of biaxially drawn samples decreases faster than that of uniaxially drawn samples, the strain-induced crystallization is expected to occur at a lower draw ratio than

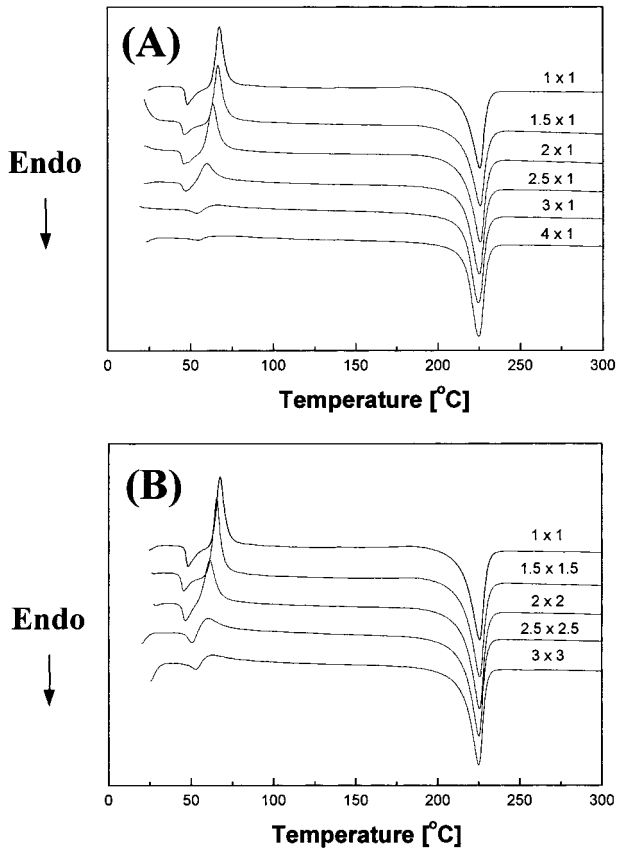

Figure 3. DSC thermograms of uniaxially (A) and biaxially (B) drawn PTMT films.

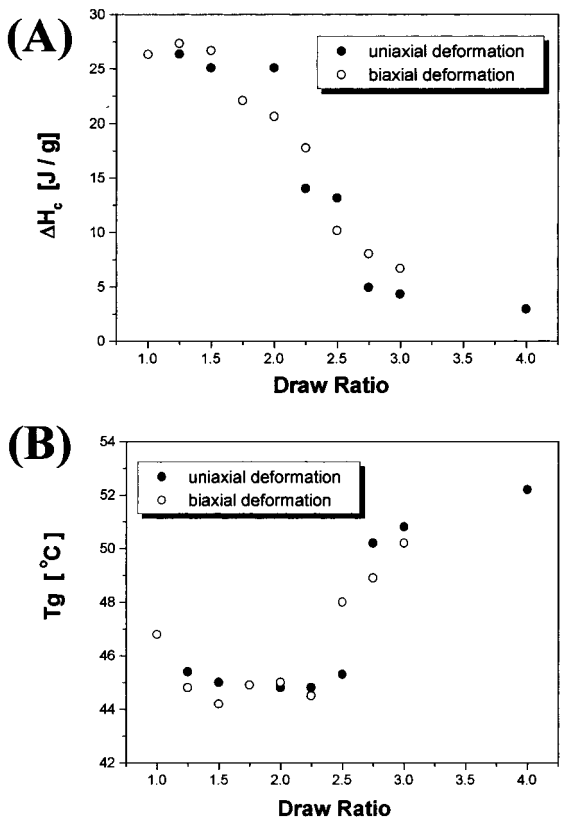

Figure 4. Crystallization enthalpy (A) and the glass transition temperature (B) as a function of draw ratio for uniaxially and biaxially drawn PTMT films.

that of uniaxially drawn samples. However, the maximum densities attained by both methods are comparable. It is to be noted that for uniaxially drawn samples the abrupt increase of the density happens at the onset of the region III in Figure 1. This result indicates that the strain hardening phenomenon in region III of Figure 1 is mainly caused by the strain-induced crystallization. As the strain turns amorphous material into crystallites, the stress concentration on the remaining amorphous region may be accelerated, resulting in the continued increase of the stress as shown in the region III in Figure 1.

The change of density and crystallinity upon drawing of amorphous PET sample have been reported in a number of studies.[28−30] With an increasing function of draw ratio, the initial region of slow density change and abrupt density increase followed by the asymptotic approach to the maximum density value have been also observed with amorphous PET samples.[28−30]

Thermal Analysis. In Figure 3, DSC thermograms of uniaxially (A) and biaxially(B) drawn films are plotted. Most samples show glass transition around 45−50 °C, crystallization exotherm around 60 °C, and melting endotherms at about 225 °C. Crystallization enthalpy and the glass transition temperature obtained from Figure 3 are shown in Figure 4, A and B, respectively. Both sets of samples (uniaxially and biaxially drawn) follow a similar trend for these properties. Below ca. dr = 2.5, little change has been observed with the glass transition temperature, as shown in Figure 4B. The abrupt increase of the glass transition temperature approximately at dr = 2.5 can be understood in terms of the strain-induced crystallization mentioned previously. As the strain-induced crystallization occurs, the mobility of the polymer chain in the amorphous region might be reduced, resulting in the increased glass transition temperature. The crystallization enthalpy plotted in Figure 4A as a function of draw ratio also shows an abrupt decrease approximately at dr = 2.5. Similar results have been reported with the stretched PET samples.[29] It is to be noted that the results from thermal analysis in Figure 4 are consistent with those in Figures 1 and 2.

Three Principal Refractive Indices. The refractive index of a material is determined by the speed of the electromagnetic wave in the medium and vacuum. Therefore, it may be affected by the density change of the medium for the isotropic material. For a drawn material, the chain orientation along MD, TD, and ND can be inferred from refractive indices along three principal directions, i.e., n_x, n_y, and n_z, respectively.[31,32] With three indices, the average refractive index (n_{av}) can be also obtained: $n_{av} = (n_x + n_y + n_z)/3$.

In Figure 5, three principal refractive indices and average refractive index of PTMT films drawn uniaxially as well as biaxially are shown. In the case of undrawn sample (dr = 1), three refractive indices are almost same, as expected. These results confirm that the amorphous sample obtained from quenching the compressed melt is macroscopically isotropic. The refractive indices along MD (n_x for uniaxial drawing in Figure 5A and n_x, n_y for biaxial drawing in Figure 5B) increase as an increasing function of draw ratio, whereas other refractive indices along TD and ND decrease. For the biaxially drawn films, both indices (n_x, n_y) along MD show similar values, indicating symmetric stretching along two directions in the film plane. And the decrease of n_z is more significant, compared with the correspond-

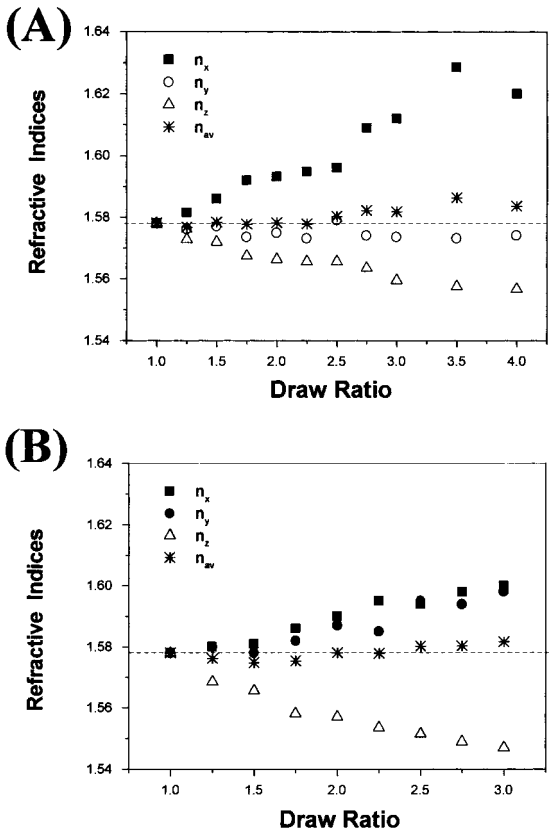

Figure 5. Three principal refractive indices as a function of draw ratio for uniaxially (A) and biaxially (B) drawn PTMT films.

ing values for uniaxial drawing. Careful examination on the results in Figure 5A would reveal close correlation between the refractive index change along MD (n_x) and the stress−strain behavior in Figure 1. While the amount of chain entanglement is reduced in region I in Figure 1, there is a small increase of the refractive index along the deformation direction, presumably due to the rotation and local slip of the chain segments which cause alignment of chain segments. As polymeric chains flow along the deformation direction in region II maintaining the stress value almost constant, the increase rate of the refractive index is reduced noticeably. Further increase of draw ratio above dr = 2.5 causes fast increase of the refractive index along the deformation direction, correlating well with the onset of the strain hardening due to the strain-induced crystallization. The stress-induced crystallization phenomenon is not clearly observed from the average refractive index, even though there is a slight increase of the average refractive at higher draw ratio, especially for the uniaxially drawn samples.

Segmental Orientation by ATR. In Figure 6, two sets of FTIR-ATR spectra of uniaxially (A) and biaxially (B) drawn PTMT films are plotted. Those spectra were obtained with the electric field direction of the infrared radiation parallel with the deformation direction (TE, *x* coordination). Four infrared bands of which band assignments are shown in Table 1 and used for the structural analysis in this work are denoted with small arrows in the figure. The band at 1410 cm^{-1} is a reference band, and all three other bands show parallel dichroism as indicated in Table 1. As the draw ratio increases, the intensity of the CH_2 wagging vibration band of the gauche conformer at 1385 cm^{-1} shows little

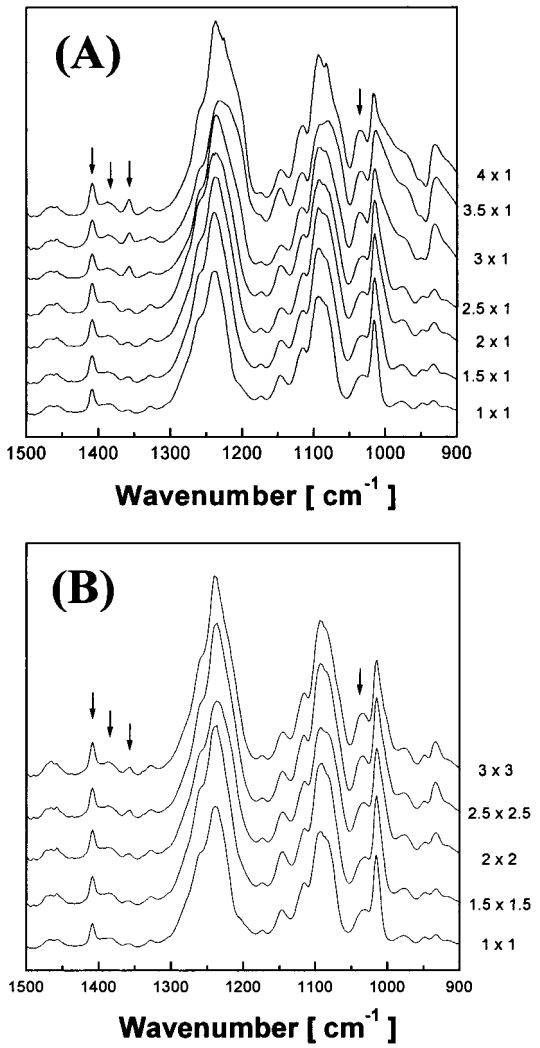

Figure 6. FTIR-ATR spectra of uniaxially (A) and biaxially (B) drawn PTMT films in TE,*x* coordinate (see text).

changes, whereas that of the trans conformer at 1358 cm^{-1} and the C−O asymmetric stretching band at 1040 cm^{-1} increases noticeably. From the spectra in Figure 6, the increase of orientation for several infrared bands along the deformation direction can be qualitatively inferred.

The attenuation indices (k_x, k_y, k_z) of the 1358 cm^{-1} band are calculated and plotted in Figures 7 as a function of draw ratio for the uniaxially drawn PTMT films. As denoted in Table 1, this band assigned to the CH_2 wagging vibration of the trans conformer shows parallel dichroism. The data in Figure 7 reveal a number of interesting points related to the orientation of the CH_2 group in the trans conformer along three spatial directions. At dr = 1, three attenuation indices have similar values, indicating that the melt quenched amorphous films are macroscopically isotropic. In a few publications on three-dimensional orientation study using the polarized FTIR-ATR method, significant differences between directions in the film plane and that normal to the plane have been reported for the undrawn films.[14−17] It is to be noted that in this work the normalized absorbance of the TM wave was multiplied with the theoretical d_e(TE)/d_e(TM) ratio to correct for the electric field amplitude difference between two polarizations. The fact that three attenuation indices have very close values at dr = 1 suggests that the

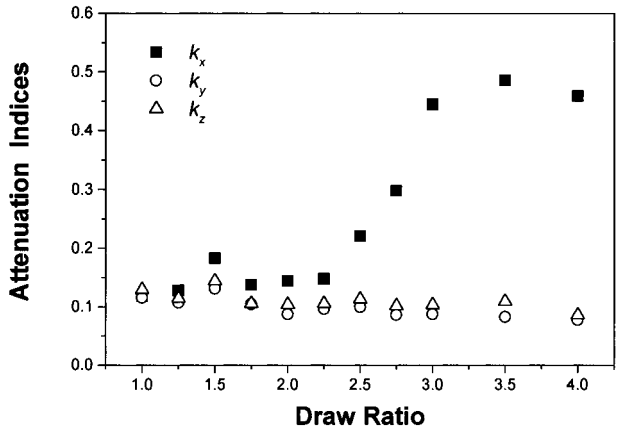

Figure 7. Attenuation indices of CH_2 wagging vibration (trans conformer, 1358 cm^{-1}) as a function of draw ratio for uniaxially drawn PTMT films.

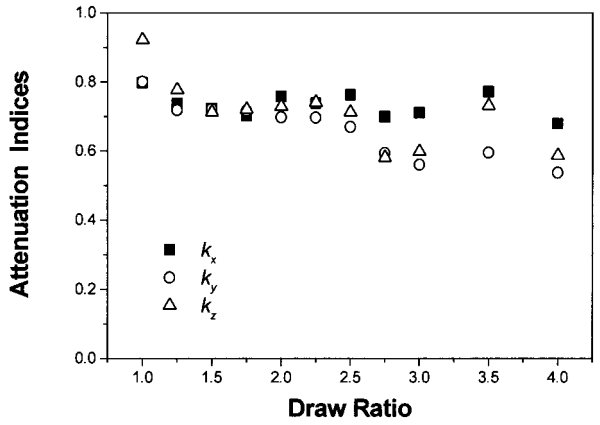

Figure 8. Attenuation indices of CH_2 wagging vibration (gauche conformer, 1385 cm^{-1}) as a function of draw ratio for uniaxially drawn PTMT films.

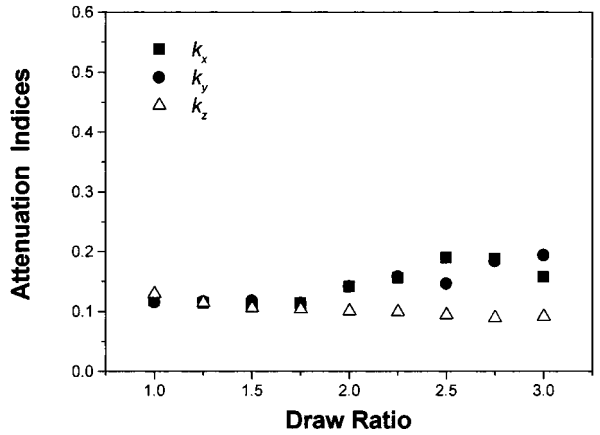

Figure 9. Attenuation indices of CH_2 wagging vibration (trans conformer, 1358 cm^{-1}) as a function of draw ratio for biaxially drawn PTMT films.

analysis method used in this work to correct for the effective thickness difference between TM and TE waves is reasonable.

With the increasing function of draw ratio, the attenuation index along the x direction (k_x) increases, in general, whereas those along two other directions tend to decrease slightly. The similarity between two values (k_y, k_z) over the whole range of draw ratios studied appears to be indicative of the cylindrical symmetry of the CH_2 group in the trans conformer along the deformation direction. As the draw ratio increases up to ca. 2.5, k_x shows a very slow increase. Further stretching above dr = 2.5 is accompanied by a sudden increase of k_x value, of which the increase rate is reduced again at ever higher draw ratio. Note that strain-induced crystallization started to occur at a draw ratio of approximately 2.5, as observed from stress−strain and density results in Figures 1 and 2, respectively. The abrupt increase of k_x at dr = 2.5 is clearly correlated with the strain-induced crystallization. These results indicate that the band at 1358 cm^{-1} is predominantly associated with the trans conformer in the crystalline region, and the CH_2 groups of trans conformers in crystallites are fairly well oriented along the deformation direction. We measured the crystal orientation of PTMT films drawn to various draw ratios with the wide-angle X-ray diffraction (WAXD) method. Well-oriented crystallites have been qualitatively verified with the X-ray results, and a detailed analysis will be carried out and reported shortly.

Figure 8 displays three attenuation indices of the 1385 cm^{-1} band which is related to the CH_2 wagging vibration of the gauche conformer. The changing trends of three attenuation indices are not so obvious as the ones in Figure 7. However, all attenuation indices seem to decrease with the increasing function of draw ratio. It is to be noted that the conformation of four bonds connected to three CH_2 units in a crystal of PTMT is trans−gauche−gauche−trans.[4,5] The amount of gauche conformation is the same as that of the trans conformation in the PTMT crystal. Therefore, the band at 1385 cm^{-1} should be more associated with the gauche conformer in the amorphous region. The increase of trans conformers in the crystalline region would be possible at the expense of the gauche conformers in the amorphous region, as expected. Note that the relative amount of gauche conformer along the x direction is slightly higher than those along the y, x directions, especially at the higher draw ratios. As mentioned in the Experimental Section, the drawing was done at about 55 °C, approximately 20 °C higher that the glass transition temperature of PTMT. Since it took about 30 s to cool the drawn film to a temperature lower than T_g of PTMT during the stretching process, the orientation relaxation might proceed for the gauche conformers in the amorphous region, resulting in the reduced difference between three attenuation indices. However, the orientation relaxation of the CH_2 group in the crystal is expected to be negligible.

Figure 9 displays attenuation indices of the 1358 cm^{-1} band of biaxially drawn PTMT films as a function of draw ratio. Note that films were stretched along x and y directions simultaneously to the same draw ratio in this work. As the draw ratio increases, attenuation indices of the 1385 cm^{-1} band along the deformation directions increase, whereas that along the normal direction decreases. Both values in the film plane show very similar behavior, thus indicating the isotropic orientation in the film plane. Fast increase of attenuation indices along the deformation directions can be again observed at draw ratio about 1.75, which is smaller than the draw ratio showing the onset of the strain-induced crystallization of uniaxially drawn films. It is clear from Figure 2 that strain-induced crystallization occurs at lower linear draw ratio for the biaxially drawn films than for the uniaxially drawn films.

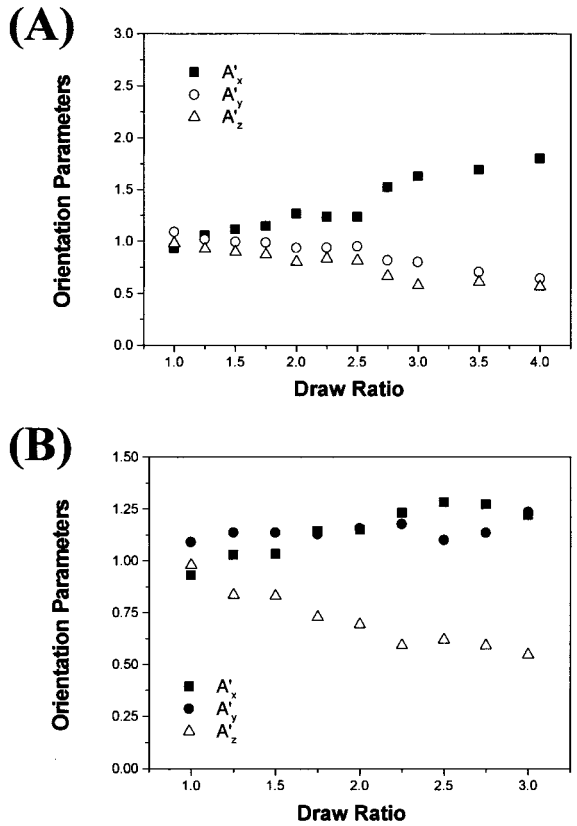

Figure 10. Spatial orientation parameters of C−O stretching vibration (1040 cm^{-1}) as a function of draw ratio for uniaxially (A) and biaxially (B) drawn PTMT films.

Three attenuation indices of the 1385 cm^{-1} band of biaxially drawn films showed a continuing decrease with the increasing function of draw ratio (data not shown). However, the decrease along the normal direction was slightly higher than the corresponding ones in the film plane. Similar to the results in Figure 8, the orientation of the gauche conformer was far less than that of the trans conformer for the biaxially drawn films. Again, orientation relaxation especially in the amorphous region might contribute to a smaller difference between three attenuation indices.

Spatial orientation parameters of the C−O stretching vibration at 1040 cm^{-1} are plotted for both uniaxially and biaxially drawn films in Figure 10. Since this band also shows parallel dichroism, the spatial orientation parameters along the deformation directions increase, and those along directions perpendicular to the deformation directions decrease with the increasing function of draw ratio. The changing behavior of A'_x with draw ratio in Figure 10 appears to be somewhat different from the corresponding values in Figures 7 and 9. The spatial orientation parameter along the deformation direction seems to increase continuously without any significant jump. A small increase at dr = 2.5 in this figure is not so obvious as that in Figure 7. Note that the band at 1358 cm^{-1} was predominantly affected by the CH_2 trans conformer in the crystalline region. The results in this figure suggest that the spatial orientation parameters of C−O stretching band at 1040 cm^{-1} are not dominated by the crystalline region of the PTMT film. If it is determined only by the overall C−O group concentration in each direction, irrespective of the morphology, then the effect of orientation on the overall spatial orientation parameter values can be separated from that of strain-induced crystallization in Figure 7. The maximum A'_x value in Figure 10A is smaller than the corresponding value in Figure 7. This fact indicates again that the band at 1040 cm^{-1} is preferentially affected by the total energy of the C−O stretching vibration both in crystalline and in amorphous regions.

The interpretation of the data in Figure 10 has to be made with some precautions. The depth of penetration (d_p), defined as the distance required for the electric field amplitude to fall to e^{-1} of its value at the interface, is given by[12]

$$d_p = \frac{\lambda_1}{2\pi(\sin^2\theta - n^2)^{1/2}} \tag{6}$$

Equation 6 indicates that the depth of penetration is proportional to the wavelength. The radiation of longer wavelength penetrates further into the film probing the bulk information more, whereas that of shorter wavelength is relatively more affected by the molecular structure at the surface. If there is a significant gradient in terms of orientation and crystallinity along the thickness direction, normalization with a band separated far from each other might introduce some error related to the depth of penetration. For the film of which orientation was introduced with the mechanical stretching, not with the melt flowing during injection into a mold, the difference between the surface and the bulk was found to be insignificant.[19] However, similar observations have to be still made with the material used in this work to justify the normalization procedure for the C−O stretching band at 1040 cm^{-1}. Another point to consider is that the C−O stretching band at 1040 cm^{-1} in Figure 6 shows appreciable overlap with the adjacent bands. Band overlap of three other bands used in this work was not so significant as the C−O stretching band at 1040 cm^{-1}. Therefore, the absorbance value of the C−O stretching band obtained from the local baseline must contain a small amount of experimental uncertainty.

Conclusions

In this work, the structural changes occurring during the stretching process have been investigated with the uniaxially and biaxially drawn PTMT films. With the stress−strain curve, DSC thermograms, and density change as a function of draw ratio, the stress-induced crystallization phenomenon have been found to happen within a narrow range of draw ratio.

The orientation of polymer chains along three principal directions in PTMT films has been measured with a polarized refractometer. The refractive indices along the deformation directions (x for uniaxilly drawn films and x, y for biaxially drawn films) increased continuously, whereas those along directions perpendicular to the deformation directions were found to decrease. The refractive index along a deformation direction for the uniaxially stretched films showed abrupt increase at draw ratio 2.5, at which the strain hardening phenomenon has been observed with the stress−strain curve.

The segmental orientation along three directions (MD, TD, ND) was also measured with polarized FTIR-ATR spectroscopy. To calculate attenuation indices along three principal directions with ATR method, the sample and ATR crystal have to be rotated by 90°. Since the symmetrically double-edged ATR crystal used in this work was found to be insufficient to ensure identical

contact between sample and ATR crystal for the four ATR setups required to calculate three-dimensional orientation information, the absorbance of a specific band was normalized with the absorbance of the reference band at 1410 cm^{-1}. Normalization with a reference band will remove the inherent intensity difference between TE and TM waves. Therefore, the absorbance of TM waves was multiplied with the theoretical effective thickness ratio $d_e(TE)/d_e(TM)$ before the attenuation indices along three directions were calculated. This method was found to give very similar attenuation indices along all three directions for isotropic PTMT sample.

The three-dimensional segmental orientation behavior was studied with three different bands of which transition dipole moment direction is parallel to the chain direction. The attenuation indices along the deformation directions (MD) of the bands studied in this work increased, while those along directions perpendicular to the deformation directions (TD, ND) were found to decrease, indicating the alignment of polymeric chains along the deformation direction. For PTMT films stretched uniaxially, the attenuation index of the 1358 cm^{-1} band (trans CH_2 conformer) along the deformation direction showed an abrupt increase approximately at $dr = 2.5$. These results were again interpreted in terms of the stress-induced crystallization. Upon stress-induced crystallization, some of the gauche conformers should be transformed into trans conformers. The transformation from gauche to trans conformers was verified with the decreasing attenuation indices of the band at 1385 cm^{-1} (CH_2 wagging of gauche conformer) along all three directions with the increasing function of draw ratio.

The orientation behavior of C−O stretching band at 1040 cm^{-1} was also studied. The spatial orientation parameters along MD directions increased continuously, whereas those along TD and ND directions decreased. With this band, the abnormal increase of orientation parameters at a specific draw ratio was not observed. This result indicates that the absorbance of this band is relatively insensitive to morphological change and mainly determined by the orientation along each direction.

Acknowledgment. This work has been supported by the INHA University research program in 1997.

References and Notes

(1) Wignall, G. D. In *Encyclopedia of Polymer Science and Engineering*, 2nd ed.; Mark, H. F., Bikales, N. M., Overberger, C. G., Menges, G., Eds.; Wiley-Interscience: New York, 1988; Vol. 12, pp 9−12.
(2) Ward, I. M.; Wilding, M. A.; Brody, H. *J. Polym. Sci., Polym. Phys. Ed.* **1976**, *14*, 263−274.
(3) Gonzalez, C. C.; Perena, J. M.; Bello, A. *J. Polym. Sci., Polym. Phys. Ed.* **1988**, *20*, 1397−1408.
(4) Poulin-Dandurand, S.; Perez, S.; Revol, J.; Brisse, F. *Polymer* **1979**, *20*, 419−426.
(5) Desborough, I. J.; Hall, I. H.; Neisser, J. Z. *Polymer* **1979**, *20*, 545−552.
(6) Bulkin, B. J.; Lewin, M.; Kim J. S. *Macromolecules* **1987**, *20*, 830−835.
(7) Kim, J. S.; Lewin, M.; Bulkin, B. J. *J. Polym. Sci., Polym. Phys. Ed.* **1986**, *24*, 1783−1789.
(8) Kim, Y. H.; Kim, K. J.; Lee, K. M. *J. Korean Fiber Soc.* **1997**, *34*, 860−867.
(9) Oh, P. R.; Kim, K. J.; Kim, Y. H. *J. Korean Fiber Soc.* **1999**, *36*, 132−139.
(10) Cole, K. C.; Guevremont, J.; Ajji, A.; Dumoulin, M. M. *Appl. Spectrosc.* **1994**, *12*, 1513−1521.
(11) Bensaad, S.; Jasse, B.; Noel, C. *Polymer* **1993**, *34*, 1602−1605.
(12) Harrick, N. J. In *Internal Reflection Spectroscopy*, 3rd ed.; Harrick Scientific Corp.: Ossining, NY, 1987.
(13) Flournoy, P. A.; Schaffers, W. J. *Spectrochim. Acta* **1966**, *22*, 5−13.
(14) Hobbs, J. P.; Sung, C. S. P.; Krishnan, K.; Hill, S. *Macromolecules* **1983**, *16*, 193−199.
(15) Sung, C. S. P.; Hobbs, J. P. *Chem. Eng. Commun.* **1984**, *30*, 229.
(16) Mirabella, F. M. *Appl. Spectrosc.* **1988**, *42*, 1258−1265.
(17) Lofgren, E. A.; Jabarin, S. A. *J. Appl. Polym. Sci.* **1994**, *51*, 1251−1267.
(18) Walls, D. J. *Appl. Spectrosc.* **1991**, *45*, 1193−1198.
(19) Walls, D. J.; Coburn, J. C. *J. Polym. Sci., Polym. Phys. Ed.* **1992**, *30*, 887−897.
(20) Kaito, A.; Nakayama, K. *Macromolecules* **1992**, *25*, 4882−4887.
(21) Everall, N. J.; Bibby, A. *Appl. Spectrosc.* **1997**, *51*, 1083−1091.
(22) Lee, H. S.; Ko, J. H.; Song, K. S.; Choi, K. H. *J. Polym. Sci., Polym. Phys. Ed.* **1997**, *35*, 1821−1832.
(23) Robinson, J. W. In *Handbook of Spectroscopy*; CRC Press: Boca Raton, FL, 1974.
(24) Ward, L. M.; Wilding, M. A. *Polymer*, **1977**, *18*, 327−335.
(25) Ouchi, I.; Hosoi, M.; Shimotsuma, S. *J. Appl. Polym. Sci.* **1977**, *21*, 3445−3456.
(26) Chandran, P.; Jabarin, S. *Adv. Polym. Technol.* **1993**, *12*, 119−132.
(27) Jabarin, S. A. *Polym. Eng. Sci.* **1992**, *32*, 1341−1349.
(28) Ajji, A.; Guevremont, J.; Cole, K. C.; Dumoulin, M. M. *Polymer* **1996**, *37*, 3707−3714.
(29) Guan, J. Y.; Wang, L. H.; Porter, R. S. *J. Polym. Sci., Polym. Phys. Ed.* **1992**, *30*, 687−691.
(30) Adams, A. M.; Buckey, C. P.; Jones, D. P. *Polymer* **2000**, *41*, 771−786.
(31) Samuels, R. J. *J. Appl. Polym. Sci.* **1991**, *26*, 1383−1412.
(32) Schael, G. W. *J. Appl. Polym. Sci.* **1964**, *8*, 2717−2722.

MA990775W